Nuclear Science and Techniques (2024) 35:61
https://doi.org/10.1007/s41365-024-01421-5

Theoretical analysis of the double-differential cross-sections of neutron, proton, deuteron, ^{3}He, and α for the p+^{6}Li reaction

Fang-Lei Zou[1,2] · Xiao-Jun Sun[1,2] · Jing-Shang Zhang[3] · Hai-Rui Guo[4] · Yin-Lu Han[2,3] · Rui-Rui Xu[3] · Xi Tao[3] · Ji-Min Wang[3] · Xiao-Dong Sun[3] · Yuan Tian[3] · Tao Ye[4] · Yong-Li Xu[2,5] · Chun-Tian Liang[2,6]

Received: 2 November 2023 / Revised: 30 December 2023 / Accepted: 7 January 2024

Abstract

Based on the unified Hauser–Feshbach and exciton model, which can describe the particle emission processes between discrete energy levels with energy, angular momentum, and parity conservations, a statistical theory of light nucleus reaction (STLN) is developed to calculate the double-differential cross-sections of the outgoing neutron and light charged particles for the proton-induced ^{6}Li reaction. A significant difference is observed between the p + ^{6}Li and p + ^{7}Li reactions owing to the discrepancies in the energy-level structures of the targets. The reaction channels, including sequential and simultaneous emission processes, are analyzed in detail. Taking the double-differential cross-sections of the outgoing proton as an example, the influence of contaminations (such as ^{1}H, ^{7}Li, ^{12}C, and ^{16}O) on the target is identified in terms of the kinetic energy of the first emitted particles. The optical potential parameters of the proton are obtained by fitting the elastic scattering differential cross-sections. The calculated total double-differential cross-sections of the outgoing proton and deuteron at E_p = 14 MeV agree well with the experimental data for different outgoing angles. Simultaneously, the mixed double differential cross-sections of ^{3}He and α are in good agreement with the measurements. The agreement between the measured data and calculated results indicates that the two-body and three-body breakup reactions need to be considered, and the pre-equilibrium reaction mechanism dominates the reaction processes. Based on the STLN model, a PLUNF code for the p + ^{6}Li reaction is developed to obtain an ENDF-6-formatted file of the double-differential cross-sections of the nucleon and light composite charged particles.

Keywords Statistical theory of light nucleus reaction · p + ^{6}Li reaction · Light composite charged particle · Double-differential cross-sections · Two-body breakup · Three-body breakup

This work was supported by the National Natural Science Foundation of China (No. 12065003), the Guangxi Key R &D Project (2023AB07029), the Scientific Research and Technology Development Project of Guilin (20210104-2), and the Central Government Guides Local Scientific and Technological Development Funds of China (Guike ZY22096024).

✉ Xiao-Jun Sun
sxj0212@gxnu.edu.cn

[1] College of Physics, Guangxi Normal University, 541004 Guilin, China

[2] Guangxi Key Laboratory of Nuclear Physics and Nuclear Technology, 541004 Guilin, China

[3] China Institute of Atomic Energy, P.O. Box 275(41), 102413 Beijing, China

[4] Institute of Applied Physics and Computational Mathematics, 10094 Beijing, China

[5] College of Physics and Electronic, Shanxi Datong University, 037009 Datong, China

[6] School of Science, Tianjin Chengjian University, 300384 Tianjin, China

1 Introduction

Nuclear data (including the cross-sections of all types of reaction channels, differential cross-sections, and double-differential cross-sections) of nucleon-induced ^{6,7}Li reactions are important for various applications, such as the compact accelerator-driven neutron source and the International

Published online: 03 May 2024

Fusion Materials Irradiation Facility (IFMIF), as introduced in Refs. [1–7]. A lithium-glass scintillator with natural lithium is used as a small-angle neutron scattering spectrometer (SANS) for material research at the China Spallation Neutron Source (CSNS) to satisfy both the neutron detection efficiency and gamma elimination requirements [8]. ^{7}Li enrichment and ^{6}Li inventory are important influencing factors in molten salt fast reactors (MSFRs) [9]. In recent years, lithium has received considerable attention in astrophysics because it can lead to a better understanding of the evolution and formation of the universe. The standard big-bang nucleosynthesis (BBN) theory overestimates the primordial ^{7}Li abundance by a factor of approximately three to four, that is, the cosmological lithium problem [10]. The reaction ^{6}Li(p, γ) ^{7}Be plays an important role in the consumption of ^{6}Li and the formation of ^{7}Be, and ^{7}Be will eventually decay into ^{7}Li at the end of big-bang nucleosynthesis [11]. In an atmosphere of approximately 1% of giant stars, there exists an anomalous elevation in lithium abundance, directly contradicting the expectations calculated by conventional stellar evolution models. An extremely Li-rich giant (possibly newly enriched) and a rigorous investigation of its evolutionary stage are definitely important [12]. Furthermore, an in-depth study of the nucleon- ^{6,7}Li reaction will enhance our understanding of 1*p*-shell light nuclear reactions [13–15].

Although ^{6}Li and ^{7}Li differ by only one neutron, they exhibit significant differences. The natural abundance of ^{6}Li is only 7.5%, whereas that of ^{7}Li is as high as 92.5%. The energy levels of ^{6}Li and ^{7}Li are different both in terms of their energy values and widths. Additionally, every energy level of the ^{6}Li nucleus has a spin with an even multiple of 1/2, whereas the spin of the ^{7}Li nucleus is an odd multiple of 1/2 [16]. ^{6}Li is easily captured by neutrons, producing ^{7}Li and high-energy gamma rays, whereas ^{7}Li is more likely to undergo α decay. Moreover, the capture cross-section of ^{6}Li is smaller than that of ^{7}Li in the thermal neutron energy range, making ^{6}Li a common material for slow neutron shielding in certain nuclear applications. Differences in the energy level diagrams of ^{6}Li and ^{7}Li can lead to variations in their decay properties and the particles emitted from the individual levels [1–6]. Therefore, the results of the n+^{6,7}Li reactions are significantly different, as shown both experimentally and theoretically [1, 2, 7]. In our previous studies, we successfully predicted the double-differential cross-sections of the charged particles for the p+^{7}Li reaction using the statistical theory of light nucleus reaction (STLN) model [15]. On this basis, an ENDF-6-formatted file of the double-differential cross-section was obtained. File-6 (file of the double-differential cross-section), one of the important files of the nuclear reaction database, is recommended when the energy and angular distributions of the emitted particles must be coupled, when it is important to provide a concurrent description of neutron scattering and particle emission, when so many reaction channels are open that it is difficult to provide separate reactions, or when accurate distributions of the charged particle or residual nucleus are required for particle transport, heat deposition, or radiation damage calculations [17]. However, there are still no publications describing the double-differential cross-sections of outgoing particles for the p+^{6}Li reaction.

Quantitatively describing all the physical quantities is challenging because of the limited availability of comprehensive experimental data for the p+^{6}Li reaction. For the p+^{6}Li reaction, there are only a small number of experimental partial cross-sections of the (p, γ), (p, el), and (p, ^{3}He) channels [18–20]. Furthermore, numerous elastic scattering angular distributions have been measured at various incident energies [20, 21]. Fortunately, the double-differential cross-sections of the outgoing proton, deuteron, and mixture of ^{3}He and α for the p+^{6}Li reaction were measured in 1989 and 1991 [22, 23]. This makes it possible to validate the theoretical calculations. The evaluated partial cross-sections of (p, el), (p, ^{3}He) and (p, *x*) are available in nuclear reaction databases such as ENDF/B-VIII.0 [24] and JENDL-5 [25]. However, the double-differential cross-sections of the outgoing neutron and charged particles were not included in these databases because the effects of the secondary particle emission processes between the discrete levels and cluster separations in light nuclear reactions have not been considered. In ENDF/B-VIII.0, the cross-sections of (p, el), (p, ^{3}He), and (p, *x*) were derived from the *R*-matrix analysis [24, 26], while in JENDL-5, multichannel *R*-matrix fitting was used to evaluate the experimental data in the incident proton energy range from 10 keV to 3 MeV. The CCONE code [25] was employed to calculate the differential cross-sections of the emitted particles in the incident proton energy range from 3 to 200 MeV. Subsequently, proton-induced reactions on ^{6,7}Li were also calculated using the CDCC method in 2013 [5], but the double-differential cross-sections of the outgoing proton, deuteron, and triton were not provided. A possible reason for this is that the sequential secondary particle emission processes were not considered in the CDCC model [6].

This study provides an in-depth analysis of the p+^{6}Li reaction based on the STLN model with energy, angular momentum, and parity conservations. The Coulomb barriers of both the incident and exit channels are considered for different charged particles. Taking an impure target as an example, the influence of contamination is described in terms of the kinetic energy. The double-differential cross-sections of the total outgoing proton, deuteron, and the mixture of ^{3}He and α are calculated by analyzing the reaction channels at different incident energies. The calculated results at $E_{\mathrm{p}} = 14$ MeV agree well with the available experimental data.

Section 2 briefly introduces the theoretical model used in this study. The reaction channels of the p+^{6}Li reaction below 20 MeV are analyzed in detail in Sect. 3. Section 4 provides a comparison between the calculated results and the experimental data, along with the corresponding analysis. A summary is provided in the final section.

2 Theoretical descriptions

2.1 Theoretical frame

Based on the unified Hauser–Feshbach and exciton model [27], which can describe the particle emission processes between the discrete energy levels with energy, angular momentum, and parity conservations, a statistical theory of light nucleus reaction (STLN) is developed to describe the mechanism of the nucleon-induced light nucleus reaction [13, 14]. A considerable amount of experimental data, with a focus on double-differential cross-sections (such as the neutron-induced reactions on ^{6}Li [1], ^{7}Li [2], ^{9}Be [28, 29], ^{10}B [30], ^{11}B [31], ^{12}C [27, 32, 33], ^{14}N [34], ^{16}O [35, 36], and ^{19}F [37] as well as the proton-induced reactions on ^{7}Li [15] and ^{9}Be [14, 38]), has been reproduced very well.

The cross-sections of the first emitted particles from the compound nucleus to the discrete energy levels of the first residual nuclei can be expressed as

$$\sigma_{m_1,k_1}(E_{\rm L}) = \sum_{j\pi} \sigma_a^{j\pi}(E_{\rm L}) \left\{ \sum_{n=3}^{n_{\max}} P^{j\pi}(n) \frac{W_{m_1,k_1}^{j\pi}(n, E^*, \varepsilon_{m_1}^{c})}{W_T^{j\pi}(n, E^*)} + Q^{j\pi}(n) \frac{W_{m_1,k_1}^{j\pi}(E^*, \varepsilon_{m_1}^{\rm c})}{W_T^{j\pi}(E^*)} \right\}, \tag{1}$$

where $P^{j\pi}(n)$ is the occupation probability of the n-th exciton state in the $j\pi$ channel, and (j and π denote the angular momentum and parity in the final state, respectively). $P^{j\pi}(n)$ can be obtained by solving the j-dependent exciton master equation under the conservation of angular momentum in pre-equilibrium reaction processes [39]. $Q^{j\pi}(n)$ is the occupation probability of the equilibrium state in the $j\pi$ channel. $W_{m_1,k_1}^{j\pi}(n, E^*, \varepsilon_{m_1}^{\rm c})$ is the emission rate of the first emitted particle m_1 in the n-th exciton state with an outgoing kinetic energy $\varepsilon_{m_1}^{c}$ in the center-of-mass system (CMS), and $W_{\rm T}^{j\pi}(n, E^*)$ is the total emission rate in the n-th exciton state. $W_{m_1,k_1}^{j\pi}(E^*, \varepsilon_{m_1}^{\rm c})$ is the emission rate of the first emitted particle m_1 in the equilibrium state with the outgoing kinetic energy $\varepsilon_{m_1}^{\rm c}$ in the CMS, and $W_{\rm T}^{j\pi}(E^*)$ is the total emission rate in the equilibrium state. E^* is the excited energy of the compound nucleus, and $\sigma_a^{j\pi}(E_{\rm L})$ is the absorption cross-section in the $j\pi$ channel. The first term of Eq. (1) inside the brackets represents the pre-equilibrium process, which is the predominant process in 1p-shell light nuclei reactions induced by the nucleon. The second term of Eq. (1) inside the brackets describes the equilibrium process.

The cross-section of the second outgoing particle from the discrete energy levels of the first residual nucleus to the discrete energy levels of the second residual nucleus can be expressed as

$$\sigma_{k_1\to k_2}(n, m_1, m_2) = \sigma_{k_1}(n, m_1) \cdot R_{m_2}^{k_1\to k_2}(E_{k_1}), \tag{2}$$

where $\sigma_{k_1}(n, m_1)$ is the cross-section of the first emitted particle, m_1 expressed in Eq. (1), and $R_{m_2}^{k_1\to k_2}(E_{k_1})$ is the branching ratio of the second outgoing particle m_2 from the energy level E_{k_1} of the first residual nucleus M_1 to the energy level E_{k_2} of the second residual nucleus M_2.

For the simultaneous emission process, for example, $a + A \to b_1 + b_2 + b_3$ (also named after the breakup reaction), the total kinetic energy $E_{\rm C}$ in the CMS can be expressed as

$$E_{\rm C} = \frac{M_A}{M_A + m_a} E_{\rm L} + Q, \tag{3}$$

where m_a and M_A are the masses of projectile particle a and target A, respectively. $E_{\rm L}$ is the incident energy, and Q is the reaction energy. In terms of the Ohlsen theory [40], the momentum distribution function of the b_1 particle with momentum $\vec{k'}_1$ in the CMS is expressed as

$$f_1(\vec{k'}_1) = \int \rho(\vec{k'}_1, \vec{k'}_2, \vec{k'}_3)\delta\left(\sum_{i=1}^{3} \vec{k'}_i\right) \delta\left(\sum_{i=1}^{3} \varepsilon_i - E_{\rm C}\right) \prod_{i=2}^{3} d\vec{k'}_i. \tag{4}$$

Where m_i denotes the mass of the b_i particle, and $\varepsilon_i = \frac{k_i'^2}{2m_i}$ denotes the kinetic energy of the b_i particle in the CMS. The δ functions represent momentum conservation and energy conservation. Assuming that the momentum distribution function ρ is a constant, that is, uniformly distributed in the momentum space. A momentum transformation can be performed as

$$\begin{aligned} \vec{p}_2 &= \vec{k'}_2, \\ \vec{p}_3 &= \vec{k'}_2 + \vec{k'}_3, \\ \vec{q}_3 &= \mu_3\left(\frac{\vec{k'}_3}{m_3} - \frac{\vec{p}_2}{M_2}\right), \end{aligned} \tag{5}$$

one can obtain the following expressions:

$$\mathrm{d}\vec{k'}_2\mathrm{d}\vec{k'}_2 = \mathrm{d}\vec{p}_3\mathrm{d}\vec{q}_3,$$
$$\frac{p_3^2}{2M_3} + \frac{q_3^2}{2\mu_3} = \frac{k_2'^2}{2m_2} + \frac{k_3'^2}{2m_3}. \tag{6}$$

Here $M_3 = m_2 + m_3,\ M_2 = m_2,\ \mu_3 = \frac{m_3 M_2}{M_3}$. Thus Eq. (4) can be rewritten as

$$f_1(\vec{k'}_1) = \rho \int \delta(\vec{p}_3 + \vec{k'}_1)\cdot \delta\left(\frac{p_3^2}{2M_3} + \frac{q_3^2}{2\mu_3} + \varepsilon_1 - E_\mathrm{C}\right)\mathrm{d}\vec{p}_3\mathrm{d}\vec{q}_3, \tag{7}$$

After performing double-vector integrations, Eq. (7) can be expressed as

$$f_1(\vec{k'}_1) = \rho 2\pi (2\mu_3)^{3/2}\sqrt{E_\mathrm{C} - \frac{M_3 + m_1}{M_3}\varepsilon_1}. \tag{8}$$

In terms of the isotropic energy spectra in the CMS, as mentioned earlier, the energy spectra of b_1 particle can be expressed using the momentum distribution function, i.e.,

$$4\pi \int N_1(\varepsilon_1)\mathrm{d}\varepsilon_1 = \int f_1(\vec{k'}_1)\mathrm{d}\vec{k'}_1 = \int f_1(\vec{k'}_1)4\pi m_1\sqrt{2m_1\varepsilon_1}\mathrm{d}\varepsilon_1. \tag{9}$$

Thus, the energy spectra of the b_1 particle with outgoing kinetic energy ε_1 or momentum $\vec{k'}_1$ in the CMS is expressed as

$$N_1(\varepsilon_1) = C_3\sqrt{\varepsilon_1\left(\varepsilon_1^{\max} - \varepsilon_1\right)}, \tag{10}$$

where $\varepsilon_1^{\max} = \frac{m_2+m_3}{m_1+m_2+m_3}E_\mathrm{C} = \frac{M-m_1}{M}E_\mathrm{C}$ denotes the maximum outgoing kinetic energy of the b_1 particle. $C_3 = \frac{8}{\pi(\varepsilon_1^{\max})^2}$ is the normalized constant given by $\int N_1(\varepsilon_1)\mathrm{d}\varepsilon_1 = 1$.

Based on the isotropic energy spectra assumption in the CMS for the three-body breakup reaction, that is, the spectra for all azimuth angles are identical, the double-differential cross-section of b_1 particle in the CMS can be expressed as

$$\frac{\mathrm{d}^2\sigma}{\mathrm{d}\Omega_1\mathrm{d}\varepsilon_1} = \frac{N_1(\varepsilon_1)}{4\pi}. \tag{11}$$

Similarly, the double differential cross-sections of b_2 and b_3 can also be expressed in the same form.

ε_C and $\mathrm{d}\Omega_\mathrm{C} = \mathrm{d}\cos\theta_\mathrm{C}\mathrm{d}\varphi_\mathrm{C}$ are used to represent the kinetic energy and azimuth angle of the b_i particle in the CMS, respectively, without losing generality. Similarly, ε_L and $\mathrm{d}\Omega_\mathrm{L} = \mathrm{d}\cos\theta_\mathrm{L}\mathrm{d}\varphi_\mathrm{L}$ are used to represent the kinetic energy and azimuth angle of the b_i particle in the LS, respectively. There is $\varphi_\mathrm{C} = \varphi_\mathrm{L}$ both in the measurements and theoretical calculations. The following relationship universally exists for the double differential cross-section in the CMS and LS:

$$\frac{\mathrm{d}^2\sigma}{\mathrm{d}\Omega_\mathrm{L}\mathrm{d}\varepsilon_\mathrm{L}}\mathrm{d}\cos\theta_\mathrm{L}\mathrm{d}\varepsilon_\mathrm{L} = \frac{\mathrm{d}^2\sigma}{\mathrm{d}\Omega_\mathrm{C}\mathrm{d}\varepsilon_\mathrm{C}}\mathrm{d}\cos\theta_\mathrm{C}\mathrm{d}\varepsilon_\mathrm{C}. \tag{12}$$

According to the Jacobian determinant of the coordinate transformation, the double-differential cross-section of the b_i particle in the laboratory system (LS) is expressed as [41]

$$\frac{\mathrm{d}^2\sigma}{\mathrm{d}\Omega_\mathrm{L}\mathrm{d}\varepsilon_\mathrm{L}} = \sqrt{\frac{\varepsilon_\mathrm{L}}{\varepsilon_\mathrm{C}}}\frac{\mathrm{d}^2\sigma}{\mathrm{d}\Omega_\mathrm{C}\mathrm{d}\varepsilon_\mathrm{C}},$$
$$\varepsilon_\mathrm{C} = \varepsilon_\mathrm{L} + \frac{m_a m_i}{(m_a + M_A)^2}E_\mathrm{L} - \frac{2\sqrt{m_a m_i}}{m_a + M_A}\sqrt{E_\mathrm{L}\varepsilon_\mathrm{L}}\cos\theta_\mathrm{L}. \tag{13}$$

Equations (10–13) have been validated in our previous studies, such as $\mathrm{n}+{}^6\mathrm{Li} \to {}^7\mathrm{Li}^* \to \mathrm{n}+\mathrm{d}+\alpha$ [1], $\mathrm{n}+{}^7\mathrm{Li} \to {}^8\mathrm{Li}^* \to \mathrm{n}+\mathrm{t}+\alpha$ [2], and $\mathrm{p}+{}^7\mathrm{Li} \to {}^8\mathrm{Be}^* \to \mathrm{p}+\mathrm{t}+\alpha$ [15].

2.2 Coulomb barrier

Owing to the effect of the Coulomb barrier [42, 43], the kinetic energy of the first outgoing charged particle $\varepsilon_{m_1}^\mathrm{c}$ must be higher than that of the Coulomb barrier V_Coul, that is, $\varepsilon_{m_1}^\mathrm{c} > V_\mathrm{Coul}$. The reduced penetration factor calculated using the optical model potential must be 0 if $\varepsilon_{m_1}^\mathrm{c} < V_\mathrm{Coul}$. Assuming a spherical nucleus [13], V_Coul can be approximated as

$$V_\mathrm{Coul} = \frac{e^2 Z_{M_1}Z_{m_1}}{r_\mathrm{C}\left(A_{M_1}^{\frac{1}{3}} + A_{m_1}^{\frac{1}{3}}\right)}, \tag{14}$$

where Z_{M_1}, A_{M_1} and Z_{m_1}, A_{m_1} are the charge and mass number of the residual nucleus and first outgoing charged particle, respectively. r_C=1.2−1.5 fm is the charge radius. For the charge radii of the proton, deuteron, triton, ^{3}He, α, and ^{5}He, the experimental data presented in Ref. [44] are used.

Therefore, the incident energy E_p must satisfy the following equation for open reaction channels:

$$E_\mathrm{p} > \frac{M_\mathrm{C}}{M_\mathrm{T}}\left(\frac{M_\mathrm{C}}{M_1}V_\mathrm{Coul} + E_{k_1} + B_1 - B_\mathrm{p}\right), \tag{15}$$

where M_C, M_T, and M_1 are the masses of the compound, target, and first residual nuclei, respectively, after the first particle is emitted. E_{k_1} denotes the excited energy of the k-th discrete level of the first residual nucleus. B_1 is the binding energy of the first particle emitted into the compound nucleus. B_p is the binding energy of the incident particle in the compound nucleus. Clearly, the Coulomb barrier can significantly affect the open reaction channels.

2.3 Particle identification

To conveniently describe the expression of the $A(a, b)B$ reaction, some quantities are defined as follows: A, B, a, and b are the target nucleus, residual nucleus, incident particle, and emitted particle, respectively. The target nucleus A is fixed in the LS, so the kinetic energy and momentum are 0, respectively. The reaction value Q is thus expressed as follows:

$$Q = E_b + E_B - E_a, \tag{16}$$

where E_b, E_B, and E_a are the kinetic energies of b, B, and a in the LS, respectively. A schematic of momentum conservation in the nuclear reactions in the LS is shown in Fig. 1, and the momentum conservation is expressed as

$$\boldsymbol{p}_a = \boldsymbol{p}_B + \boldsymbol{p}_b, \tag{17}$$

where $p_a = \sqrt{2m_aE_a}$, $p_b = \sqrt{2m_bE_b}$, and $p_B = \sqrt{2m_BE_B}$ are the momenta of a, b, and B in the LS, respectively. Furthermore, m_a, m_b, and m_B are the masses of a, b and B, respectively.

From Eqs. (16) and (17), the kinetic energy of the first emitted particle b in the LS can be expressed as

$$E_b = \left\{ \frac{(A_aA_bE_a)^{1/2}}{A_b + A_B}\cos\theta \pm \left[\left(\frac{A_B - A_a}{A_b + A_B} + \frac{A_aA_b}{(A_B + A_b)^2}\cos^2\theta\right)E_a + \frac{A_B}{A_B + A_b}Q\right]^{1/2} \right\}^2, \tag{18}$$

3 Analysis of the reaction channels

For the proton-induced ^{6}Li reaction, reaction channels theoretically exist at an incident energy $E_p \le 20$ MeV in terms of the reaction threshold energy E_{th} as follows:

$$\mathrm{p} + {}^6\mathrm{Li} \to {}^7\mathrm{Be}^* \to \begin{cases} (\mathrm{p},\gamma)^7\mathrm{Be}, & Q = +5.606\,\mathrm{MeV}, & E_{th} = 0.000\,\mathrm{MeV} \\ (\mathrm{p,n})^6\mathrm{Be}, & Q = -5.071\,\mathrm{MeV}, & E_{th} = 5.9206\,\mathrm{MeV} \\ (\mathrm{p,p})^6\mathrm{Li}, & Q = 0.000\,\mathrm{MeV}, & E_{th} = 0.000\,\mathrm{MeV} \\ (\mathrm{p},{}^3\mathrm{He})\alpha, & Q = +4.019\,\mathrm{MeV}, & E_{th} = 0.000\,\mathrm{MeV} \\ (\mathrm{p,d})^5\mathrm{Li}, & Q = -3.442\,\mathrm{MeV}, & E_{th} = 4.0187\,\mathrm{MeV} \\ (\mathrm{p,np})^5\mathrm{Li}, & Q = -5.666\,\mathrm{MeV}, & E_{th} = 6.6153\,\mathrm{MeV} \\ (\mathrm{p,pn})^5\mathrm{Li}, & Q = -5.666\,\mathrm{MeV}, & E_{th} = 6.6153\,\mathrm{MeV} \\ (\mathrm{p,2p})^5\mathrm{He}, & Q = -4.594\,\mathrm{MeV}, & E_{th} = 5.3637\,\mathrm{MeV} \\ (\mathrm{p,pd})^4\mathrm{He}, & Q = -1.475\,\mathrm{MeV}, & E_{th} = 1.7221\,\mathrm{MeV} \\ (\mathrm{p,dp})^4\mathrm{He}, & Q = -1.475\,\mathrm{MeV}, & E_{th} = 1.7221\,\mathrm{MeV}. \end{cases} \tag{19}$$

From Eq. (19), one can see that there are obvious differences in the p+^{7}Li reaction, as shown in Eq. (12) in Ref. [15]. For the first particle emission processes, the p+^{6}Li reaction lacks the (p, t) and (p, α) channels. For the second-particle emission process, the p+^{6}Li reaction lacks the (p, nα + αn), (p, 2n), (p, nd+dn), and (p, pt+tp) channels. Furthermore, the threshold energies of the same channels are different.

Considering the energy, angular momentum, and parity conservations in the particle emission processes, the reaction channels for the first particle emission are as follows:

$$\mathrm{p} + {}^6\mathrm{Li} \to {}^7\mathrm{Be}^* \to \begin{cases} \mathrm{n} + {}^6\mathrm{Be}^* & (k_1 = gs, 1), \\ \mathrm{p} + {}^6\mathrm{Li}^* & (k_1 = gs, 1, 2, 3, 4, 5), \\ \mathrm{d} + {}^5\mathrm{Li}^* & (k_1 = gs, 1), \\ {}^3\mathrm{He} + \alpha, \end{cases} \tag{20}$$

where k_1 denotes the energy levels of the first residual nuclei, M_1, and gs denotes the ground state. Their energy-level schemes are taken from the experiments in Refs. [16, 45, 46].

For the first particle emission channel ^{6}Li(p, n)^{6}Be*, the first residual nucleus ^{6}Be* that reaches the first energy level can still emit a proton with the second residual nucleus ^{5}Li*. Furthermore, the second residual nucleus ^{5}Li* can emit a proton and alpha through the direct two-body breakup process, thus contributing to the (p, n2pα) reaction channel.

For the first particle emission channel ^{6}Li(p, p)^{6}Li*, the second excited energy level ($E_{k_1=2} = 3.563$ MeV) of the residual nucleus ^{6}Li cannot emit any particle because the parity is not conserved; thus, this reaction process purely contributes to the inelastic scattering channel. The first and third excited energy levels of ^{6}Li can emit a deuteron, so they contribute to the (p, pdα) reaction channel. If the first residual nucleus ^{6}Li* is in the k_1-th ($k_1 \ge 4$) excited energy level, some energy levels will emit a proton with the second residual nucleus ^{5}He*. Furthermore, the second residual nucleus ^{5}He* can emit a neutron and alpha from the direct two-body breakup process, thereby contributing to the (p, n2pα) reaction channel. If the first residual nucleus ^{6}Li* is in the k_1-th ($k_1 \ge 4$) excited energy level, some energy levels can also emit a deuteron, so these reaction processes contribute to the (p, pdα) reaction channel. Therefore, the first

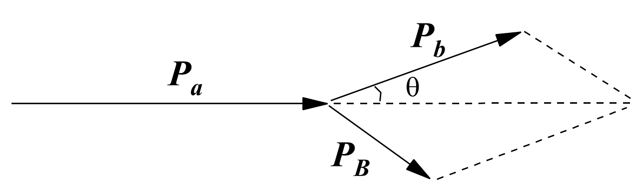

Fig. 1 Schematic of the momentum conservation in the nuclear reactions in LS

particle emission channel ^{6}Li(p, p)^{6}Li* can contribute to the (p, n2pα) and (p, pdα) reaction channels in the final state besides the elastic and inelastic channels.

For the first particle emission channel, ^{6}Li(p, d)^{5}Li*, the reaction process $^5\mathrm{Li}^* \rightarrow \mathrm{p} + \alpha$ occurs as mentioned above, so this reaction channel belongs to the (p, dpα) reaction channel in the final state. For the first outgoing ^{3}He from the compound nucleus to the ground state of the first residual nucleus α, this process only contributes to the (p, ^{3}He) α reaction channel.

According to the analyses of the reaction channels discussed above, the total spectra can be determined by adding all the partial spectra of the same outgoing particle obtained from every reaction channel. The contributions to the double-differential cross-sections of the total emitted protons are from elastic scattering, inelastic scattering, direct three-body breakup, and the (p,n2pα) and (p,pdα) reaction channels. The contributions to the double-differential cross-sections of the total emitted deuterons are from (p, d)^{5}Li*, (p, pdα), and the direct three-body breakup process $^7\mathrm{Be}^* \rightarrow \mathrm{p} + \mathrm{d} + \alpha$. The contributions to the double-differential cross-sections of the total emitted alpha are only from (p, ^{3}He)α, (p, n2pα), (p, pdα), and the direct three-body breakup process $^7\mathrm{Be}^* \rightarrow \mathrm{p} + \mathrm{d} + \alpha$. The contribution to the double-differential cross-section of the total emitted ^{3}He is only from the (p, ^{3}He)α reaction channel. It is worth mentioning that the experimental double-differential cross-sections are a mixture of ^{3}He and α because of the difficulties encountered in the measurement [22].

In conclusion, for the proton-induced ^{6}Li reaction, reaction channels finally exist at an incident energy $E_\mathrm{p} \leq 20$ MeV as follows:

$$
\mathrm{p} + {}^6\mathrm{Li} \rightarrow {}^7\mathrm{Be}^*
$$

$$
\rightarrow \begin{cases}
\mathrm{n} + {}^6\mathrm{Be}^* \begin{cases} k_1 = gs & & (\mathrm{p,\ n}) \\ k_1 = 1 & \mathrm{p} + {}^5\mathrm{Li}^* \rightarrow \mathrm{p} + \alpha & (\mathrm{p,\ n2p}\alpha) \end{cases} \\
\mathrm{p} + {}^6\mathrm{Li}^* \begin{cases} k_1 = gs & \text{Compound elastic} & \\ k_1 = 2 & & (\mathrm{p,\ p'}) \\ k_1 = 4, 5 & \mathrm{p} + {}^5\mathrm{He}^* \rightarrow \mathrm{n} + \alpha & (\mathrm{p,\ n2p}\alpha) \\ k_1 = 1, 3, 4, 5 & \mathrm{d} + \alpha & (\mathrm{p,\ pd}\alpha) \end{cases} \\
\mathrm{d} + {}^5\mathrm{Li}^* \quad k_1 = gs, 1 \quad \mathrm{p} + \alpha \quad (\mathrm{p,\ pd}\alpha) \\
{}^3\mathrm{He} + \alpha \quad (\mathrm{p,\ {}^3He}) \\
\mathrm{p} + \mathrm{d} + \alpha \quad \text{three-body breakup} \quad (\mathrm{p,\ pd}\alpha).
\end{cases} \tag{21}
$$

4 Calculated results

The experimental double-differential cross-sections of light charged particles (proton, deuteron, ^{3}He, and α) for the p+^{6}Li reaction were measured in Refs. [22, 23]. Based on the STLN model, a PLUNF code for the p+^{6}Li reaction is developed to calculate the double-differential cross-sections of the outgoing nucleon and light composite charged particles. Comparisons are performed between the calculations and measurements of the double-differential cross-sections for the total outgoing proton, deuteron, ^{3}He, and alpha particles for the p+^{6}Li reaction.

Because the target is contaminated by ^{1}H, ^{7}Li, ^{12}C, and ^{16}O, there are additional contributions to the double-differential cross-sections. Using Eq. (18), the kinetic energies of the outgoing proton and its residual nuclei from the ground state to the fifth energy level of the pure ^{6}Li and contaminants are identified. For example, for the double-differential cross-sections of the outgoing proton at an angle of 60° at E_p = 14 MeV in the LS, as shown in Fig. 2a, the black narrow bands in the below panel (b) represent the contributions of the outgoing proton from the discrete levels (only illustrated from ground state to the fifth energy level, as marked) of targets ^{6}Li and contaminants (including ^{1}H, ^{7}Li, ^{12}C, and ^{16}O). From Fig. 2, one can see that the contributions to the first abrupt peak on the right-hand side are the elastic scattering of protons with ^{12}C and ^{16}O. The contributions to the second peak on the right-hand side are the elastic scattering of protons with ^{6}Li and ^{7}Li, and the first inelastic scattering of ^{7}Li. The contribution to the third peak on the right-hand side is the pure inelastic scattering of protons with the first excited energy level of ^{6}Li. The contributions to the first peak on the left-hand side are the elastic scattering of protons with ^{1}H, the inelastic scattering of protons from the third to the fifth excited energy level of ^{12}C, and the fifth excited energy level of ^{7}Li. The levels of ^{7}Li exhibit clear differences in their contributions to the double-differential cross-section of the outgoing protons compared with those of ^{6}Li.

Comparisons of the calculated double-differential cross-sections of the total outgoing proton with the measured data are shown in Figs. 3, 4 and 5 at an incident proton energy of 14 MeV for outgoing angles of 20°, 30°, 40°, 50°, 60°, 70°, 80°, 90°, 100°, 110°, 120°, 130°, 140°, 150°, 160°, and 165°. The black points represent the experimental data obtained from Ref. [23], and the red solid lines denote the calculated total double-differential cross-sections of the outgoing proton. One can see that the calculated results agree well with the measurements, except for some peaks contaminated by elastic and inelastic scattering from ^{1}H, ^{7}Li, ^{12}C, and ^{16}O, as reported in Ref. [23]. Taking the calculated double-differential cross-sections of the outgoing proton with 60° at E_p = 14 MeV as an example, the partial spectra are shown in Fig. 6. The yellow dash-dotted line denotes the partial spectra of the proton emitted from a direct three-body breakup through $^7\mathrm{Be}^* \rightarrow$ p+d+α. The pink dash-dotted lines denote the partial spectra of the first outgoing proton from the compound nucleus to the ground state and the fifth excited

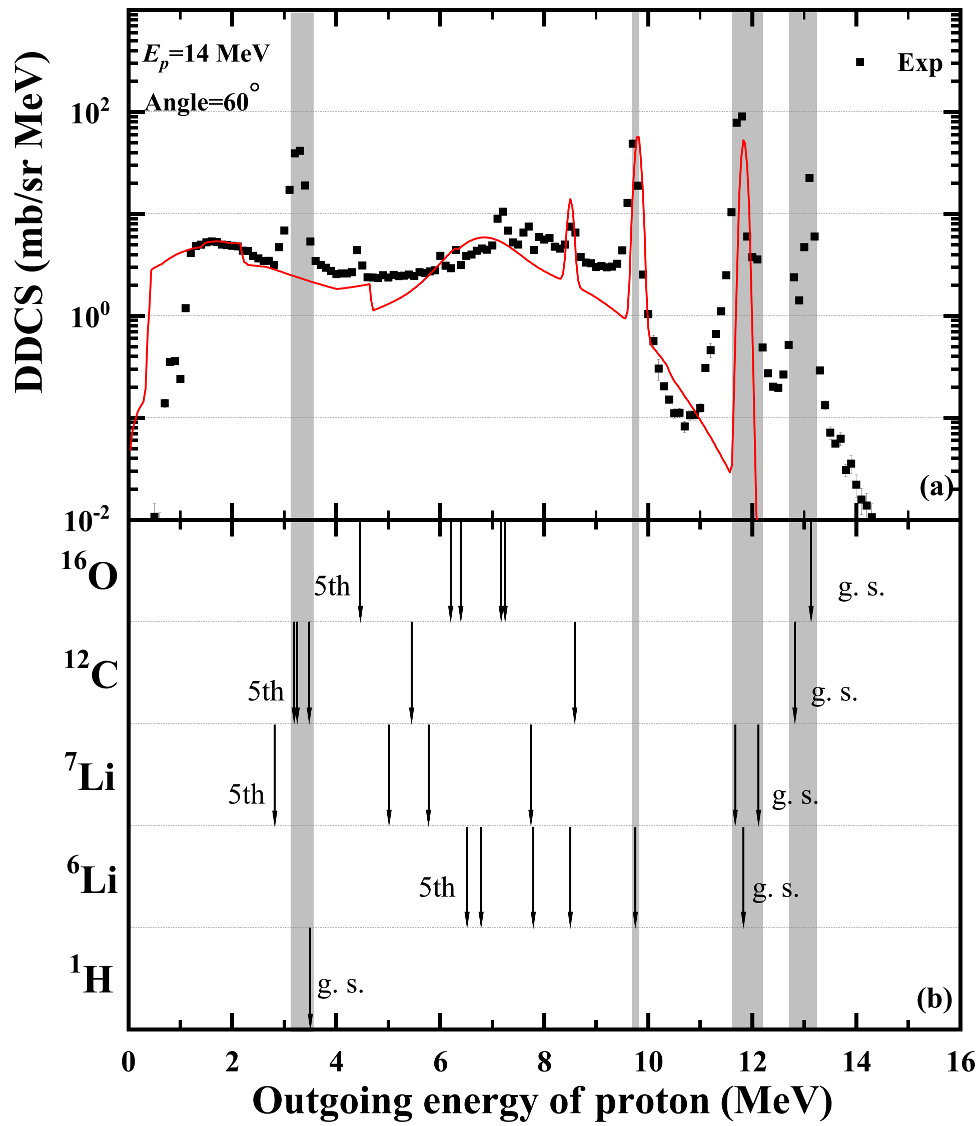

Fig. 2 (Color online) Measured and calculated total double-differential cross-sections of the outgoing proton for a proton-induced impure ^{6}Li reaction with an angle of 60° at E_{p} = 14 MeV in LS (**a**). The experimental data are obtained from Ref. [23]. The black narrow bands of the below panel (**b**) represent the contributions of the outgoing proton from the discrete levels (only illustrated from ground state to the fifth energy level as marked) of targets ^{6}Li and contaminants (including ^{1}H, ^{7}Li, ^{12}C, and ^{16}O)

energy levels of the first residual nucleus, ^{6}Li*. The green dash-dotted line represents the contribution of the reaction channel (p, np)^{5}Li* → (p, n2p)α from the first excited energy level of ^{6}Be* to the first excited energy level of ^{5}Li*, which can be broken up into p+α. The brown dash-dotted lines denote the partial spectra of the second outgoing proton from the fourth and fifth excited energy levels of ^{6}Li* to the ground state of ^{5}He*. The purple dash-dotted lines denote the partial spectra of the second outgoing proton from the ground state and the first excited energy levels of ^{5}Li* to the ground state of ^{4}He. As the target is contaminated by ^{1}H, ^{7}Li, ^{12}C, and ^{16}O, there are additional contributions to the double-differential cross-sections besides the target nucleus ^{6}Li. The energy levels of the contaminants contribute more to the lower outgoing energy regions as the outgoing angle increases, resulting in theoretical underestimations of the outgoing proton in these regions.

The calculated double-differential cross-sections of the total outgoing deuteron for the p+^{6}Li reaction at 14 MeV are compared with the experimental data obtained at angles of 20°, 30°, 40°, 50°, 60°, 70°, 80°, 90°, 100°, 110°, 120°, 130°, 140°, 150°, 160°, and 165°, as shown in Figs. 7, 8, 9, and 10. The black points represent the experimental data obtained from Ref. [22], and the red solid lines denote the calculated total double-differential cross-sections of the outgoing deuteron. Figure 10 shows the partial double-differential cross-sections of the outgoing deuteron with an angle of 60° at E_{p} = 14 MeV in the LS. The yellow dash-dotted line denotes the partial spectra of the emitted deuteron from a direct three-body breakup through ^{7}Be* → p+d+α. The green dash-dotted lines denote the partial spectra of the first outgoing deuteron from the

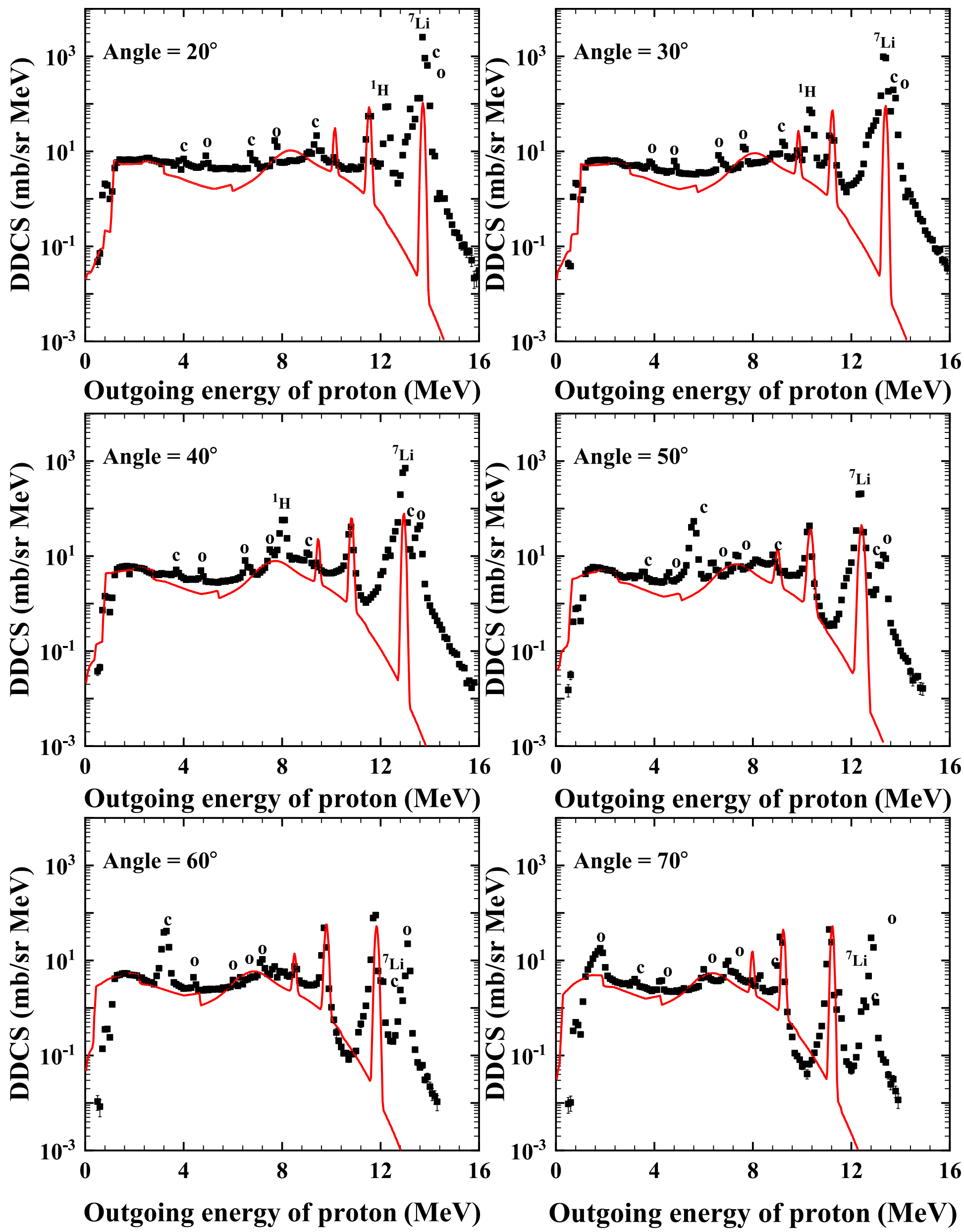

Fig. 3 (Color online) Total double-differential cross-sections of the outgoing proton for the p + ^{6}Li reaction with angles of 20°, 30°, 40°, 50°, 60°, and 70° at E_p = 14 MeV in LS. The black points denote the experimental data taken from Ref. [23]. The red solid lines denote the calculated results. The abrupt peaks represent the contributions from the contaminants, such as ^{1}H, ^{7}Li, ^{12}C, and ^{16}O. The different outgoing angles are indicated in the figure

compound nucleus to the ground state and the first excited energy levels of the first residual nucleus, ^{5}Li*. The pink dash-dotted lines denote the second outgoing deuteron from the first and the third-fifth excited energy levels of ^{6}Li* to the ground state of ^{4}He.

The calculated double-differential cross-sections of the total outgoing ^{3}He and α for the p+^{6}Li reaction at 14 MeV are compared with the experimental data obtained at angles of 10°, 20°, 30°, 40°, 50°, 60°, 70°, 80°, 90°, 100°, 110°, and 120°, as shown in Figs. 11, 12. The black points represent the experimental data obtained from Ref. [22], and the red solid lines denote the calculated total double-differential cross-sections. The calculated results agree well with the measurements. From Fig. 13, one can see that the yellow dash-dotted line denotes the partial spectra of the emitted α from the direct three-body breakup process through ^{7}Be* → p+d+α. The green dash-dotted line denotes the contribution of the reaction channel (p, np)^{5}Li* → (p, n2p)α from the first excited energy level of ^{6}Be* to the first excited energy level of ^{5}Li*, which can be broken up into p+α. The pink dash-dotted lines denote the second outgoing α from the first and third–fifth excited energy levels of ^{6}Li* to the ground state of ^{4}He. The blue dash-dotted lines denote the partial spectra of the first outgoing ^{3}He from the compound nucleus to the ground state of the first residual nucleus α. One can see that the first and second peaks on the right-hand side are the differential cross-sections of the outgoing ^{3}He and α for p+

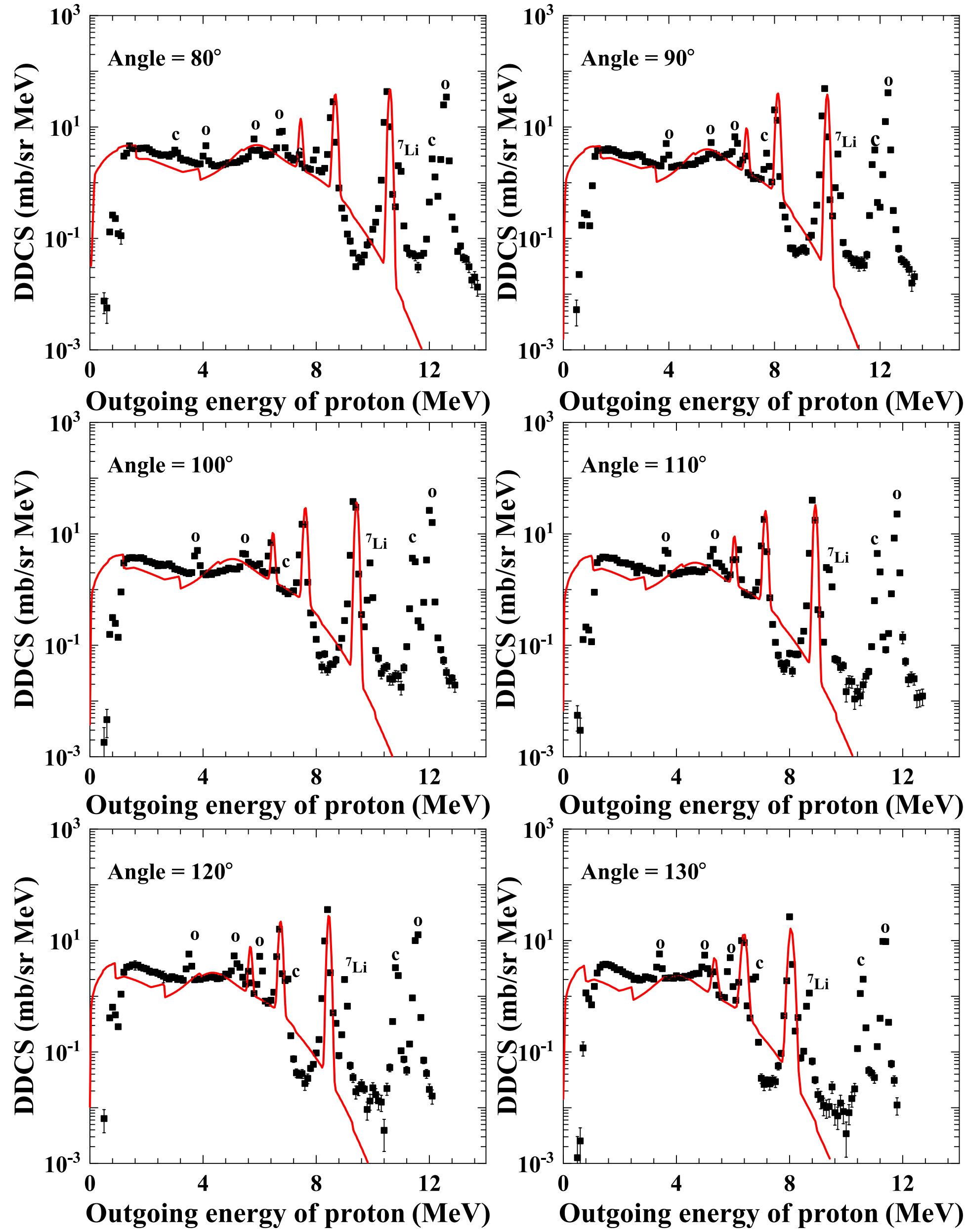

Fig. 4 (Color online) Same as Fig. 3, but at outgoing angles of 80°, 90°, 100°, 110°, 120°, and 130°

^{6}Li, respectively. In particular, p+^{6}Li $\rightarrow$^{3}He + α is different from a secondary particle emission because it has no threshold. It is worth mentioning that the peaks are marked incorrectly in Figs. 11, 12 of Ref. [22]. The purple dash-dotted lines denote the partial spectra of the second outgoing α from the ground state and the first excited energy levels of ^{5}Li* to the ground state of ^{4}He.

As an example, Fig. 14 shows the predicted total and partial spectra of the outgoing neutron for the p+^{6}Li reaction at 14 MeV at an angle of 60°. The red line shows the total double-differential cross-sections of the outgoing neutron. The green dash-dotted lines denote the partial spectra of the first outgoing neutron from the compound nucleus to the ground state and the first excited energy level of the first residual nucleus, ^{6}Be*. The brown dash-dotted lines denote the contribution of the reaction (p, 2p)^{5}He $\rightarrow$ (p, n2p)α from the fourth and fifth excited energy levels of ^{5}He* to the ground state of α.

However, the threshold energies of composite charged particles, such as deuteron and triton (except ^{3}He and alpha for the p+^{6}Li reaction), are usually higher than those of the protons for both the target and contaminants. Furthermore, the Coulomb barriers of these outgoing composite charged particles are higher than those of the protons; therefore, the impact of the contaminants is greatly reduced. These factors hinder the accurate measurement of these composite charged particles, particularly at larger outgoing angles. Thus, it is reasonable to

Fig. 5 (Color online)Same as Fig. 3, but at outgoing angles of 140°, 150°, 160°, and 165°

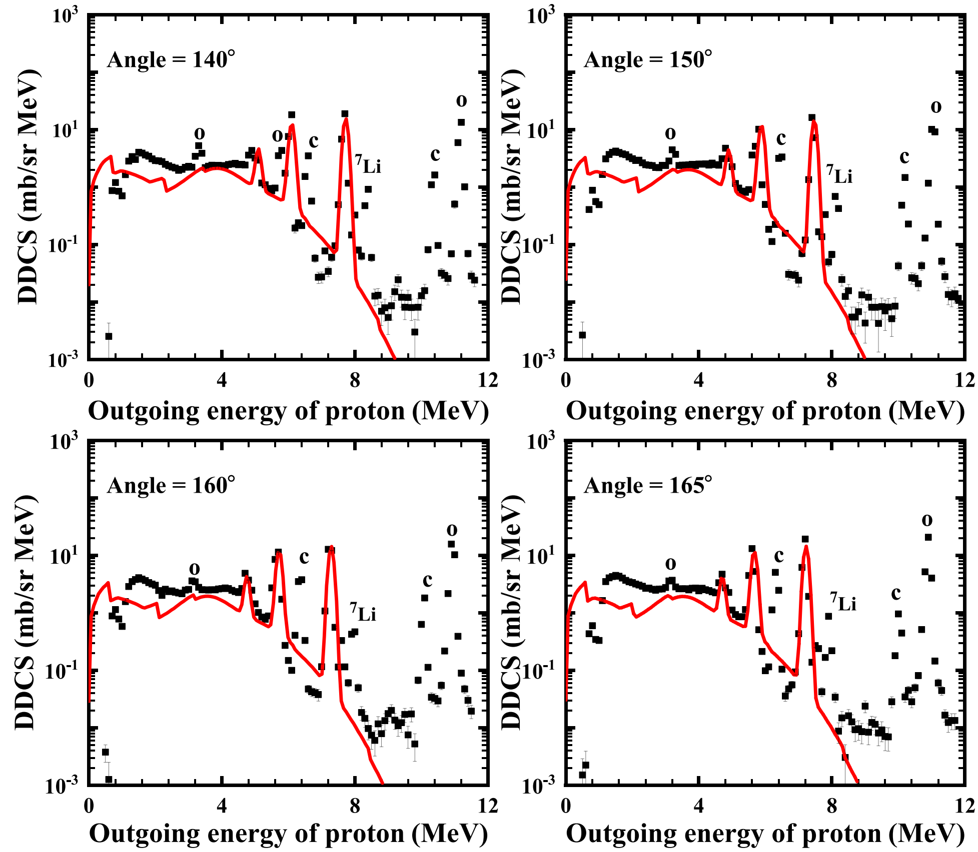

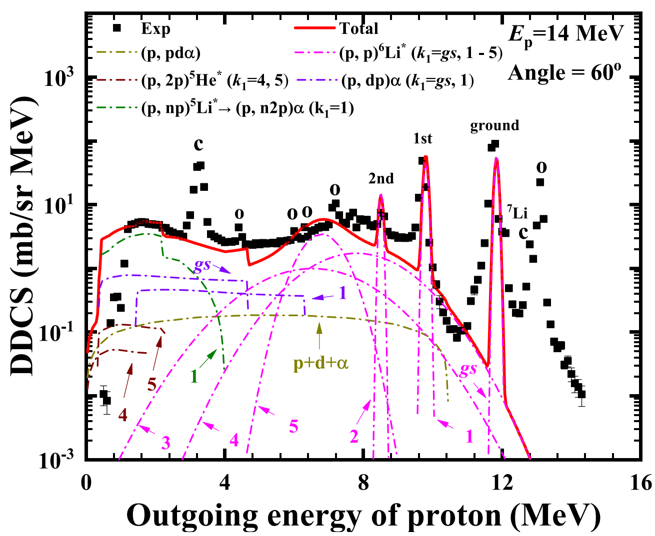

Fig. 6 (Color online) Partial double-differential cross-sections of the outgoing proton from the p+^{6}Li reaction with an outgoing angle of 60° at E_p = 14 MeV in LS. The black points denote the experimental data taken from Ref. [23], and the red solid line denotes the calculated total double-differential cross-sections. The yellow dash-dotted line denotes the partial spectra of the emitted proton from the direct three-body breakup through ^{7}Be* → p+d+α. The pink dash-dotted lines denote the partial spectra of the first outgoing proton from the compound nucleus to the fifth excited energy levels of the first residual nucleus, ^{6}Li*. The green dash-dotted line denotes the contribution of the reaction channel (p, np)^{5}Li* → (p, n2p)α from the first excited energy level of ^{6}Be* to the first excited energy level of ^{5}Li*, which can break up into d+α. The brown dash-dotted lines denote the partial spectra of the second outgoing proton from the fourth and fifth excited energy levels of ^{6}Li* to the ground state of ^{5}He*. The purple dash-dotted lines denote the partial spectra of the second outgoing proton from the ground state and the first excited energy level of ^{5}Li* to the ground state of ^{4}He

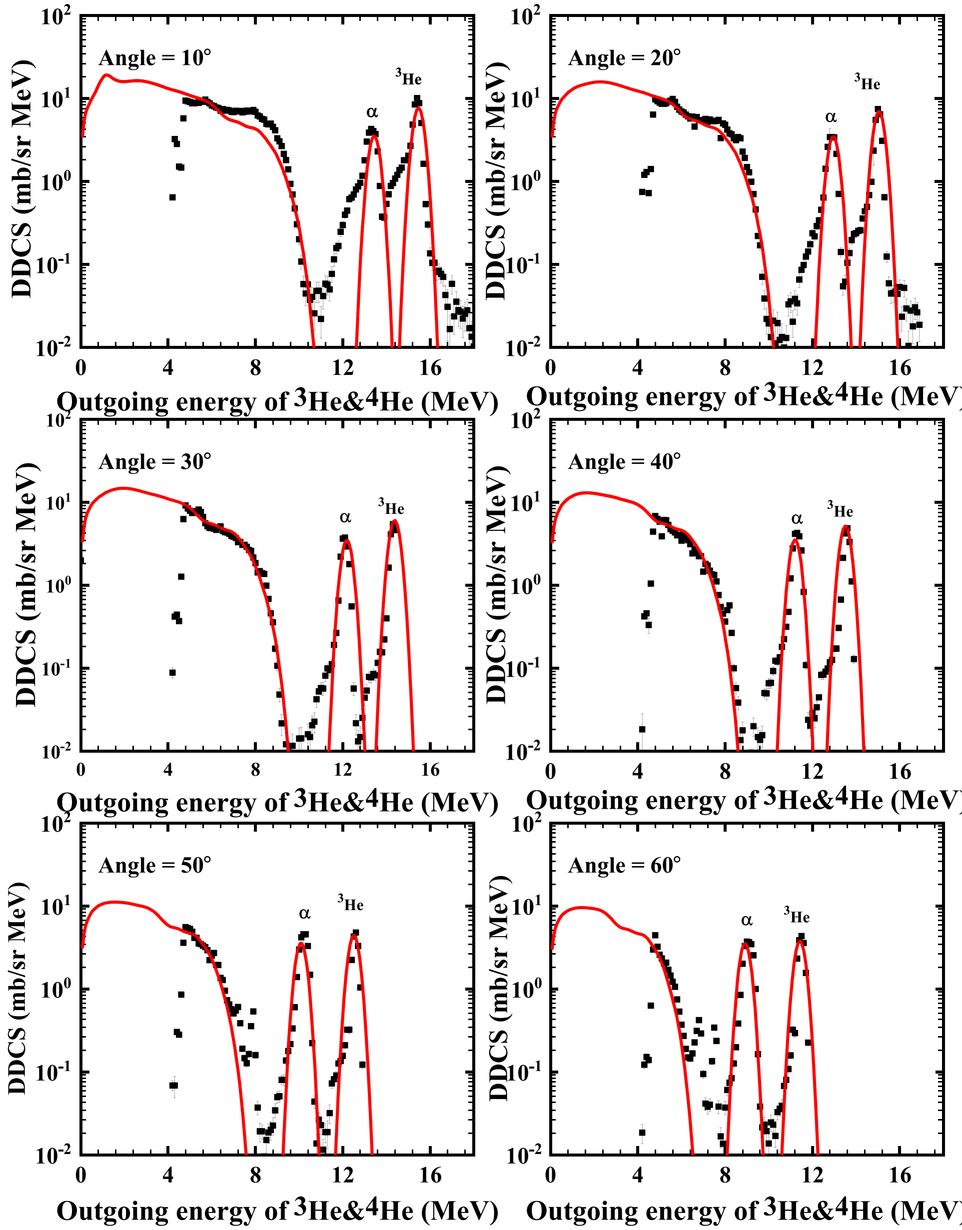

Fig. 7 (Color online) Same as Fig. 3, but for outgoing ^{3}He and α particles. The experimental data are taken from Ref. [22]

assume that the theoretical calculations are slightly higher than those of the measurements for large outgoing angles.

5 Summary

The STLN model [39, 47, 48] is improved to calculate the double-differential cross-sections of outgoing neutrons, protons, deuterons, ^{3}He, and alpha particles for the p+^{6}Li reaction. The emission processes between discrete energy levels with energy, angular momentum, and parity conservations are strictly considered. The results show that the pre-equilibrium emission process is the dominant reaction mechanism for 1p-shell light nucleus reactions and that the calculated double-differential cross-sections are sensitive to the energy, spin, and parity of the discrete levels for both the target and residual nuclei. Recoiling effects are also considered owing to the light mass of the 1p-shell nuclei. A PLUNF code is developed based on the STLN model to obtain an ENDF-6-formatted file of the double-differential cross-sections of the nucleon and light composite charged particles for the p+^{6}Li reaction. The

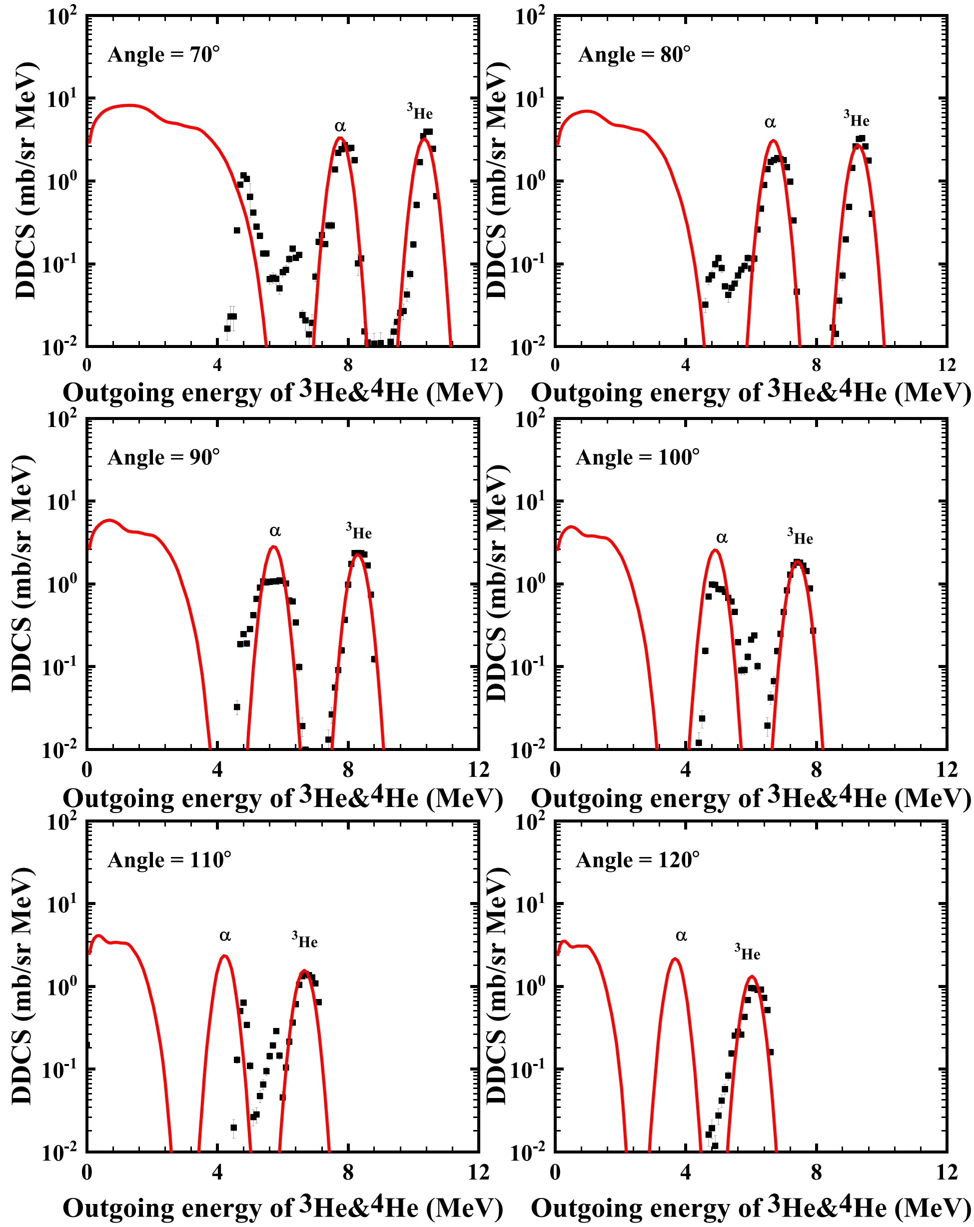

Fig. 8 (Color online) Same as Fig. 7, but for different outgoing angles, which are marked in the figure

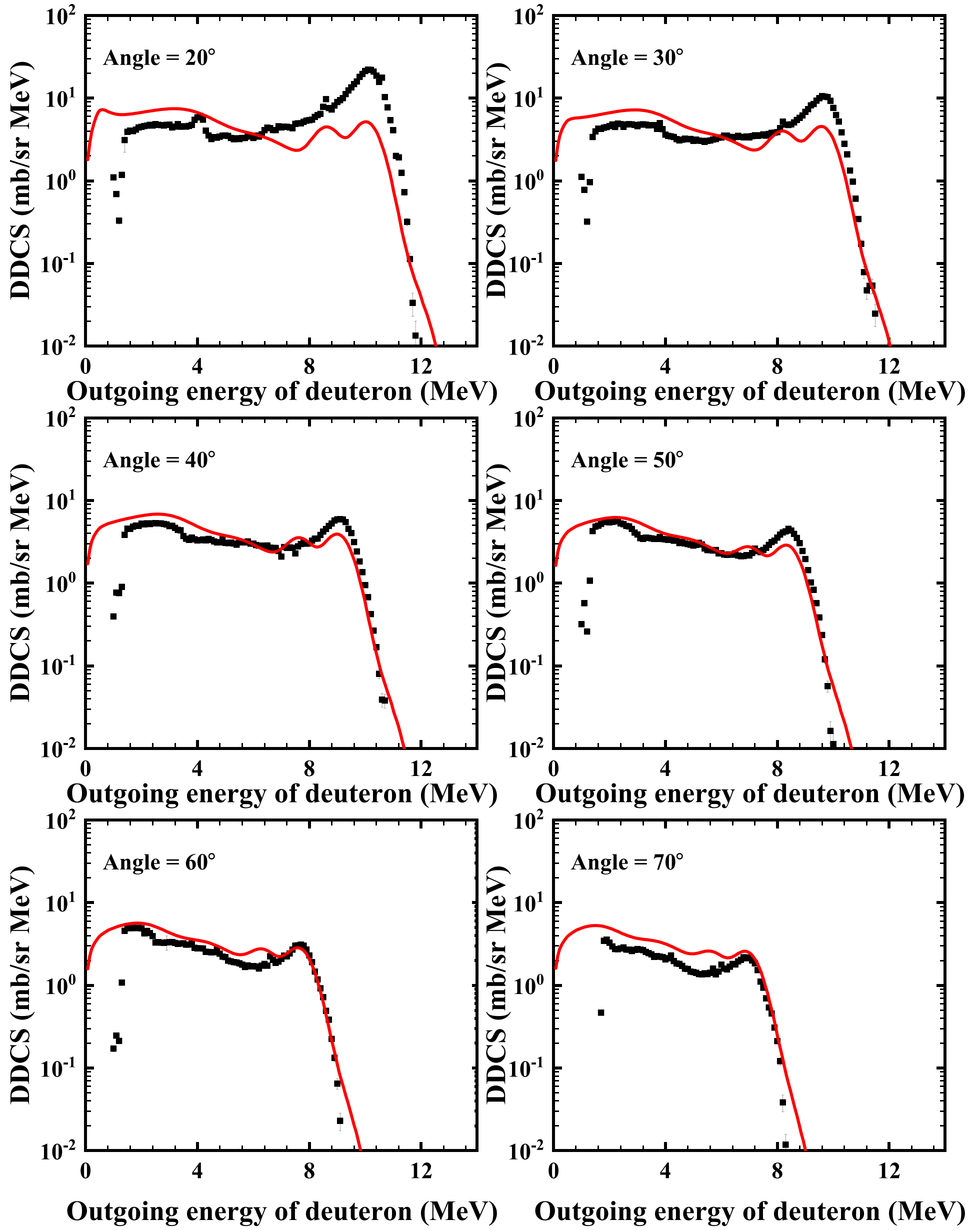

Fig. 9 (Color online) Same as Fig. 3, but for the outgoing deuteron. The experimental data are taken from Ref. [22]

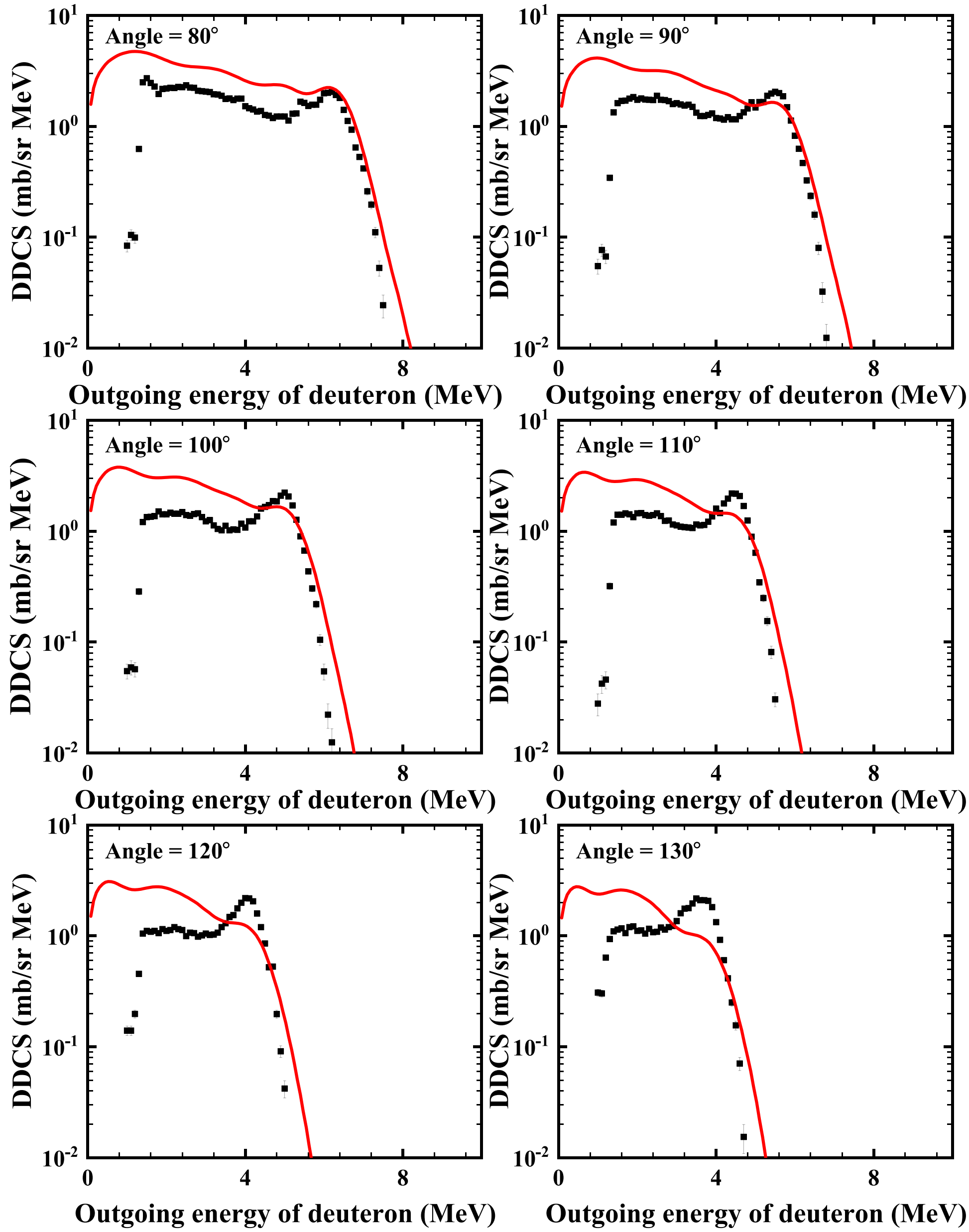

Fig. 10 (Color online) Same as Fig. 9, but for different outgoing angles, which are marked in the figure

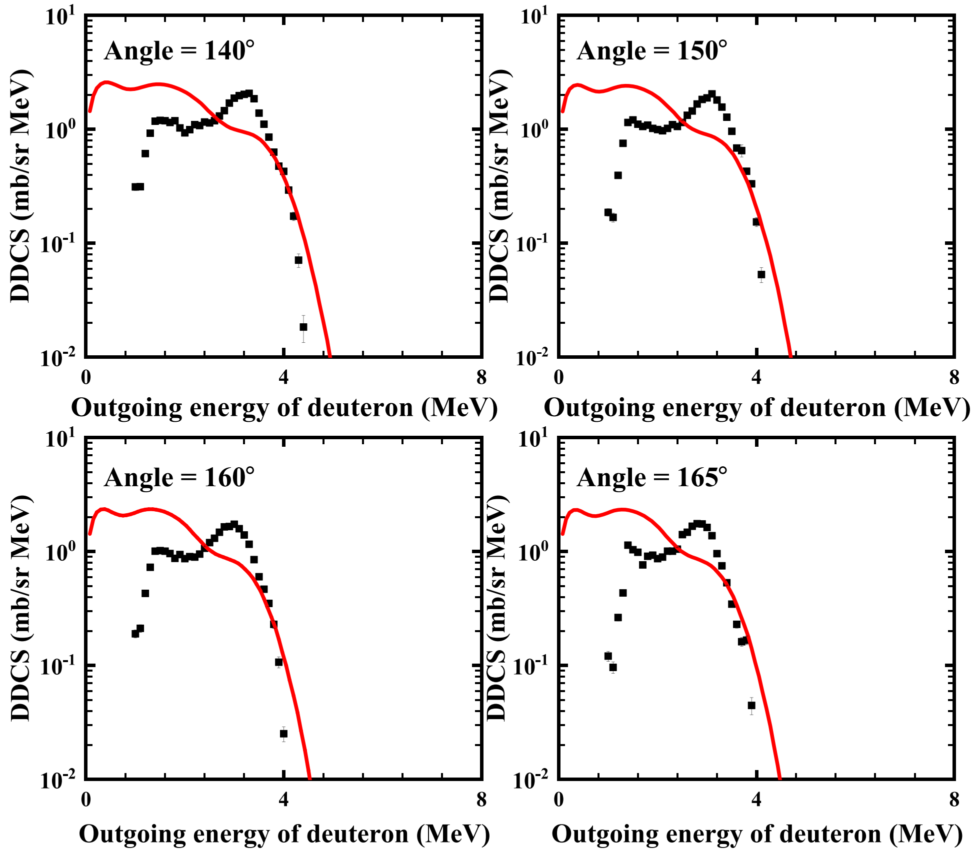

Fig. 11 (Color online) Same as Fig. 9, but for different outgoing angles, which are marked in the figure

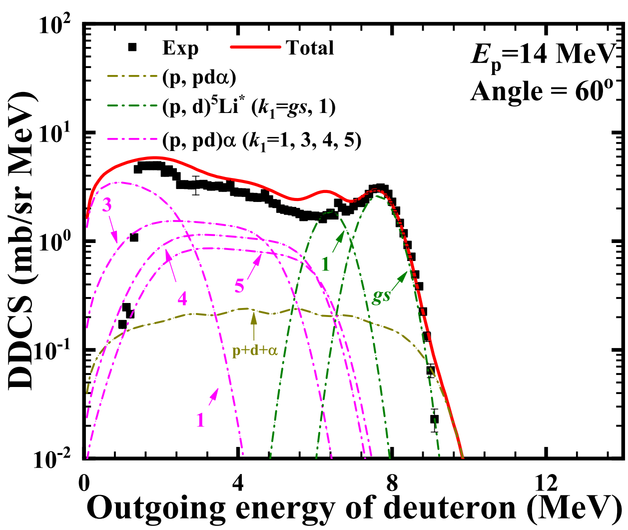

Fig. 12 (Color online) Same as Fig. 6, but for the outgoing deuteron. The yellow dash-dotted line denotes the partial spectra of the emitted deuteron from direct three-body breakup through ^{7}Be* → p+d + α. The green dash-dotted lines denote the partial spectra of the first outgoing deuteron from the compound nucleus to the ground state and the first excited energy level of the first residual nucleus, ^{5}Li*. The pink dash-dotted lines denote the second outgoing deuteron from the first and third–fifth excited energy levels of ^{6}Li* to the ground state of ^{4}He

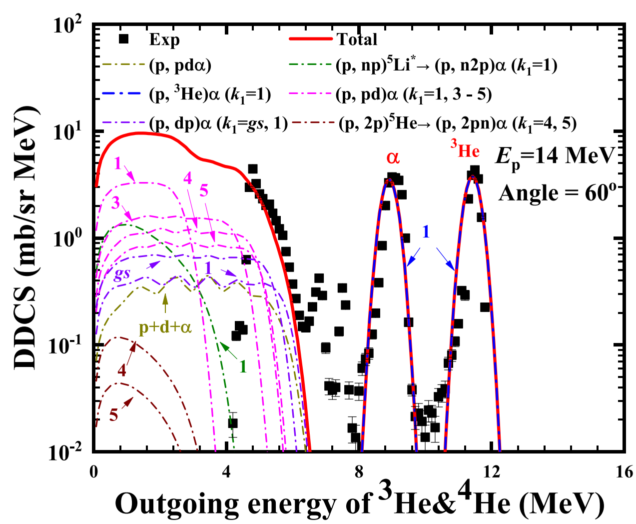

Fig. 13 (Color online) Same as Fig. 6, but for outgoing ^{3}He and α. The yellow dash-dotted line denotes the partial spectra of the emitted α from direct three-body breakup through ^{7}Be* → p+d + α. The green dash-dotted line denotes the contribution of the reaction channel (p, np)^{5}Li* → (p, n2p)α from the first excited energy level of ^{6}Be* to the first excited energy level of ^{5}Li*, which can break up into d+α. The pink dash-dotted lines denote the second outgoing α from the 1st and 3rd–5th excited energy levels of ^{6}Li* to the ground state of ^{4}He. The blue dash-dotted lines denote the partial spectra of the first outgoing ^{3}He from the compound nucleus to the ground state of the first residual nucleus α. The purple dash-dotted lines denote the partial spectra of the second outgoing α from the ground state and first excited energy levels of ^{5}Li* to the ground state of ^{4}He

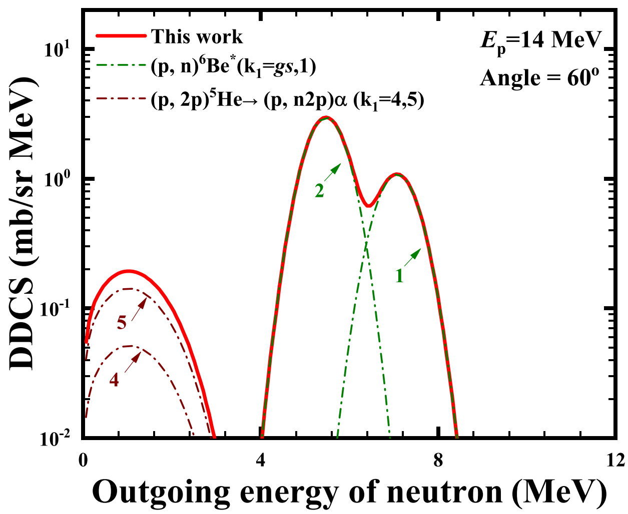

Fig. 14 (Color online) The predicted total and partial double-differential cross-sections of the outgoing neutron from the p+^{6}Li reaction with an outgoing angle of 60° at E_p = 14 MeV in the LS. The green dash-dotted lines denote the partial spectra of the first outgoing neutron from the compound nucleus to the ground state and the first excited energy level of the first residual nucleus, ^{6}Be*. The brown dash-dotted lines denote the contribution of the reaction (p, 2p)^{5}He → (p, n2p) α from the fourth and fifth excited energy levels of ^{5}He* to the ground state of α

calculated results agree well with existing measurements of outgoing protons, deuterons, ^{3}He, and alpha particles.

Author contributions All authors contributed to the study conception and design. Material preparation, data collection and analysis were performed by Xiao-Jun Sun, Fang-Lei Zou and Jing-Shang Zhang. The first draft of the manuscript was written by Xiao-Jun Sun,Fang-Lei Zou and all authors commented on previous versions of the manuscript. All authors read and approved the final manuscript.

Declarations

Conflict of interest The authors declare that they have no Conflict of interest.

References

1. J.S. Zhang, Y.L. Han, Model calculation of n + ^{6}Li reactions below 20 MeV. Commun. Theor. Phys. **36**, 437 (2001). https://doi.org/10.1088/0253-6102/36/4/437
2. J.S. Zhang, Y.L. Han, Calculation of double-differential cross sections of n + ^{7}Li reactions below 20 MeV. Commun. Theor. Phys. **37**, 465 (2002). https://doi.org/10.1088/0253-6102/37/4/465
3. T. Matsumoto, D. Ichinkhorloo, Y. Hirabayashi et al., Systematic description of the ^{6}Li(n, n')^{6}Li* → d + α reactions with the microscopic coupled-channels method Phys. Rev. C **83**, 064611 (2011). https://doi.org/10.1103//PhysRevC.83.064611
4. D. Ichinkhorloo, Y. Hirabayashi, K. Kato et al., Analysis of ^{7}Li(n, n')^{7}Li* reactions using the continuum-discretized coupled-channels method. Phys. Rev. C **86**, 064604 (2012). https://doi.org/10.1103/PhysRevC.86.064604
5. H.R. Guo, Y. Watanabe, T. Matsumoto et al., Systematic analysis of nucleon scattering from ^{6,7}Li with the continuum discretized coupled channels method. Phys. Rev. C **87**, 024610 (2013). https://doi.org/10.1103/physrevc.87.024610
6. H.R. Guo, Y. Watanabe, T. Matsumoto et al., Analysis of nucleon and triton emissions from nucleon-^{7}Li collisions below 20 MeV. Phys. Rev. C **99**, 034602 (2019). https://doi.org/10.1103/physrevc.99.034602
7. H.Y. Bai, R.R. Fan, H.Y. Jiang et al., Measurement of the differential cross sections and angle-integrated cross sections of the ^{6}Li(n, t)^{4}He reaction from 1.0 eV to 3.0 MeV at the CSNS Back-n white neutron source. Chin. Phys. C **44**, 014003 (2020). https://doi.org/10.1088/1674-1137/44/1/014003
8. K. Zhou, J.R. Zhou, Y.S. Song et al., Compact lithium-glass neutron beam monitor for SANS at CSNS. Nucl. Sci. Tech. **29**, 127 (2018). https://doi.org/10.1007/s41365-017-0250-7
9. G.C. Li, Y. Zou, C.G. Yu et al., Influence of ^{7}Li enrichment on Th-U fuel breeding for an Improved Molten Salt Fast Reactor (IMSFR). Nucl. Sci. Tech. **28**, 97 (2017). https://doi.org/10.1007/s41365-018-0468-z
10. J.J. He, Cosmological lithium problem. Chin. Sci. Bull. **65**, 4047 (2020). https://doi.org/10.1360/TB-2020-0951
11. S.B. Dubovichenko, A.S. Tkachenko, R.Y. Kezerashvili et al., ^{6}Li(n,γ)^{7}Be reaction rate based on new data from the Laboratory for Underground Nuclear Astrophysics. Phys. Rev. C **105**, 065806 (2022)
12. H.L. Yan, J.R. Shi, Y.T. Zhou et al., The nature of the lithium enrichment in the most Li-rich giant star. Nat. Astron. **2**, 10 (2018). https://doi.org/10.1038/s41550-018-0544-7
13. J.S. Zhang, *Statistical Theory of Neutron Induced Reactions of Light Nuclei*, 2nd edn. (Science Press, Beijing, 2015). (**in Chinese**)
14. X.J. Sun, J.S. Zhang, Statistical theory of light-nucleus reactions and application to the ^{9}Be(p, xn) reaction. Phys. Rev. C **93**, 014609 (2016). https://doi.org/10.1103/PhysRevC.93.014609
15. J.Q. Hu, X.J. Sun, J.S. Zhang et al., Theoretical analysis of double-differential cross sections of proton, deuteron, and triton emission in the p + ^{7}Li reaction at 14 MeV. Phys. Rev. C **101**, 034616 (2020). https://doi.org/10.1103/PhysRevC.101.034616
16. D.R. Tilley, C.M. Cheves, J.L. Godwin et al., Energy levels of light nuclei A = 5, 6, 7. Nucl. Phys. A **708**, 3–163 (2002). https://doi.org/10.1016/S0375-9474(02)00597-3
17. A. Trkov, M. Herman, D.A. Brown, et al., ENDF-6 formats manual: Data formats and procedures for the evaluated nuclear data files. (2018). https://doi.org/10.2172/1425114
18. J.J. He, S.Z. Chen, C.E. Rolfs et al., A drop in the ^{6}Li(p, γ) reaction at low energies. Phys. Lett. B **725**, 287–291 (2013). https://doi.org/10.1016/j.physletb.2013.07.044
19. C.R. Gould, R.O. Nelson, J.R. Williams et al., Cross-section requirements for charged-particle fusion reactors: the ^{6}Li(p, ^{3}He)α reaction. Nucl. Sci. Eng. **55**, 267–272 (1974). https://doi.org/10.13182/nse74-a23453
20. M. Haller, M. Betz, W. Kretschmer et al., Elastic scattering of polarized protons by ^{6}Li: (I) Optical-model analysis. Nucl. Phys. A **496**, 189–204 (1989). https://doi.org/10.1016/0375-9474(89)90171-1
21. W.D. Harrison, A.B. Whitehead, Elastic scattering of protons by ^{6}Li. Phys. Rev. (1963). https://doi.org/10.1103/PhysRev.132.2607
22. N. Koori, I. Kumabe, M. Hyakutake et al., Prlarized proton induced reactions on lithium isotopes around 14 MeV. JEARI-M 91-009 (1991). https://doi.org/pdfdata/JAERI-M-91-009.pdf

23. N. Koori, I. Kumabe, M. Hyakutake et al., Prlarized proton scatter on lithium isotopes at 14 MeV. JEARI-M 89-167 (1989). https://doi.org/publications/indc/indc-jpn-0130.pdf
24. A.D. Carlson, V.G. Pronyaev, R. Capote et al., Evaluation of the neutron data standards. Nucl. Data Sheets **148**, 143–188 (2018). https://doi.org/10.1016/j.nds.2018.02.002
25. O. Iwamoto, Extension of a nuclear reaction calculation code CCONE toward higher incident energies - multiple preequilibrium emission, and spectrum in laboratory system. J. Nucl. Sci. Technol. **50**, 409–418 (2013). https://doi.org/10.1080/00223131.2013.773168
26. P.R. Page, G.M. Hale, ^{8}Be nuclear data evaluation. AIP Conf. Proc. **769**, 390–393 (2005). https://doi.org/10.1063/1.1945030
27. J.S. Zhang, Y.L. Han, L.G. Cao, Model calculation of n + ^{12}C reactions from 4.8 to 20 MeV. Nucl. Sci. Eng. **133**, 218–234 (1999). https://doi.org/10.13182/NSE98-100
28. J.F. Duan, J.S. Zhang, H.C. Wu et al., Predicted levels of ^{9}Be based on a theoretical analysis of neutron double-differential cross sections at E_n = 14.1 and 18 MeV. Phys. Rev. C **80**, 064612 (2009). https://doi.org/10.1103/PhysRevC.80.064612
29. J.F. Duan, J.S. Zhang, H.C. Wu et al., Theoretical analysis of neutron double-differential cross sections of n + ^{9}Be reactions. Commun. Theor. Phys. **54**, 129 (2010). https://doi.org/10.1088/0253-6102/54/1/25
30. J.S. Zhang, Theoretical analysis of neutron double-differential cross section of n + ^{10}B at 14.2 MeV. Commun. Theor. Phys. **39**, 433 (2003). https://doi.org/10.1088/0253-6102/39/4/433
31. J.S. Zhang, Theoretical analysis of neutron double-differential cross section of n + ^{11}B at 14.2 MeV. Commun. Theor. Phys. **39**, 83 (2003). https://doi.org/10.1088/0253-6102/39/1/83
32. X.J. Sun, W.J. Qu, J.F. Duan et al., New calculation method of neutron kerma coefficients for carbon and oxygen below 30 MeV. Phys. Rev. C **78**, 054610 (2008). https://doi.org/10.1103/PhysRevC.78.054610
33. X.J. Sun, J.F. Duan, J.M. Wang et al., Analysis of neutron double-differential cross sections for n + ^{12}C reaction below 30 MeV. Commun. Theor. Phys. **48**, 534 (2007). https://doi.org/10.1088/0253-6102/48/3/02
34. Y.L. Yan, J.F. Duan, X.J. Sun et al., Analysis of neutron double-differential cross section of n + ^{14}N at 14.2 MeV. Commun. Theor. Phys. **44**, 128 (2005). https://doi.org/10.1088/6102/44/1/128
35. J.S. Zhang, Y.L. Han, X.L. Fan, Theoretical analysis of the neutron double differential cross section of n + ^{16}O at E_n = 14.1 MeV. Commun. Theor. Phys. **35**, 579 (2001). https://doi.org/10.1088/0253-6102/35/5/579
36. J.F. Duan, Y.L. Yan, J.M. Wang et al., Further analysis of neutron double-differential cross section of n + ^{16}O at 14.1 MeV and 18 MeV. Commun. Theor. Phys. **44**, 701 (2005). https://doi.org/10.1088/6102/44/4/701
37. J.F. Duan, Y.L. Yan, X.J. Sun et al., Theoretical analysis of neutron double-differential cross section of n + ^{19}F at 14.2 MeV. Commun. Theor. Phys. **47**, 102 (2007). https://doi.org/10.1088/0253-6102/47/1/020
38. X.J. Sun, J.S. Zhang, New integral formula for obtaining analytical Legendre expansion coefficients and its applications to light-nucleus reactions. Phys. Rev. C **92**, 061601(R) (2015). https://doi.org/10.1103/PhysRevC.92.061601
39. J.S. Zhang, A unified Hauser-Feshbach and exciton model for calculating double-differential cross sections of neutron-induced reactions below 20 MeV. Nucl. Sci. Eng. **114**, 55 (1993). https://doi.org/10.13182/NSE93-3
40. G.G. Ohlsen, Kinematic relations in reactions of the form A + B→C+D+E. Nucl. Inst. Methods **37**, 240–248 (1965). https://doi.org/10.1016/0029-554X(65)90368-X
41. Q.B. Shen, *Low and medium energy nuclear reaction theory*, 2nd edn. (Science Press, Beijing, 2015). (**in Chinese**)
42. G.R. Satchler, Heavy-ion scattering and reactions near the Coulomb barrier and "threshold anomalies". Physics Reports (Review Section of Physics Letters) **199**. No.3, 147-190. North-Holland (1991).https://doi.org/10.1016/0370-1573(91)90066-U
43. P.W. Riesenfeldt, T.D. Thomas, Influence of nuclear forces on the Coulomb barrier in heavy-ion reactions. Phys. Rev. C **2**, 6 (1970). https://doi.org/10.1103/PhysRevC.2.2448
44. I. Angeli, K.P. Marinova, Table of experimental nuclear ground state charge radii: An update. At. Data and Nucl. Data Tables **99**, 69–95 (2013). https://doi.org/10.1016/j.adt.2011.12.006
45. D.R. Tilley, H.R. Weller, G.M. Hale et al., Energy levels of light nuclei A = 4. Nucl. Phys. A **541**, 1 (1992). https://doi.org/10.1016/0375-9474(92)90635-W
46. D.R. Tilley, J.H. Kelley, J.L. Godwin et al., Energy levels of light nuclei A = 8, 9, 10. Nucl. Phys. A **745**, 155 (2004). https://doi.org/10.1016/j.nuclphysa.2004.09.059
47. X.J. Sun, J.S. Zhang, Statistical theory of light nucleus reactions with 1*p*-shell light nuclei. EPJ Web Conf. **146**, 12026 (2017). https://doi.org/10.1051/epjconf/201714612026
48. Y.L. Yan, J.F. Duan, J.S. Zhang et al., Double-differential cross section of ^{5}He emission. Commun. Theor. Phys. **43**, 299 (2005). https://doi.org/10.1088/0253-6102/43/2/020